

Accurate Polarimetric BRDF for Real Polarization Scene Rendering

Yuhi Kondo, Taishi Ono, Legong Sun, Yasutaka Hirasawa, and Jun Murayama

Sony Corporation, Tokyo, Japan

{Yuhi.Kondo, Taishi.Ono, Legong.Sun, Yasutaka.Hirasawa,
Jun.Murayama}@sony.com

Abstract. Polarization has been used to solve a lot of computer vision tasks such as Shape from Polarization (SfP). But existing methods suffer from ambiguity problems of polarization. To overcome such problems, some research works have suggested to use Convolutional Neural Network (CNN). But acquiring large scale dataset with polarization information is a very difficult task. If there is an accurate model which can describe a complicated phenomenon of polarization, we can easily produce synthetic polarized images with various situations to train CNN.

In this paper, we propose a new polarimetric BRDF (pBRDF) model. We prove its accuracy by fitting our model to measured data with variety of light and camera conditions. We render polarized images using this model and use them to estimate surface normal. Experiments show that the CNN trained by our polarized images has more accuracy than one trained by RGB only.

Keywords: polarization, shape from polarization, polarimetric BRDF, convolutional neural network

1 Introduction

Polarization is the property of light that is invisible to human unlike brightness or color. In the field of computer vision, various works utilizing polarization effect have been studied. In the early years, polarization had been used to remove or separate reflection components of an image [21]. From the beginning of 2000, several studies related to Shape from Polarization (SfP) [1][3][5][19][20] and Bidirectional Reflectance Distribution Function (BRDF) including polarization property [23][31] were proposed. In 2016, an image sensor which implement a polarizer on each pixel with different angles was developed [37], and it enabled a single shot capture of polarized images of 0° , 45° , 90° , 135° . Since then, the number of studies related to SfP increased [7][8], however these studies still suffer from the following two critical problems.

First, there is an ambiguity between polarization angle x and $x + 180^\circ$ which results in the ambiguity of azimuth angle in SfP.

Second problem is that there are two kinds of reflection which are specular reflection and diffuse reflection. Many studies ignore diffuse reflection assuming

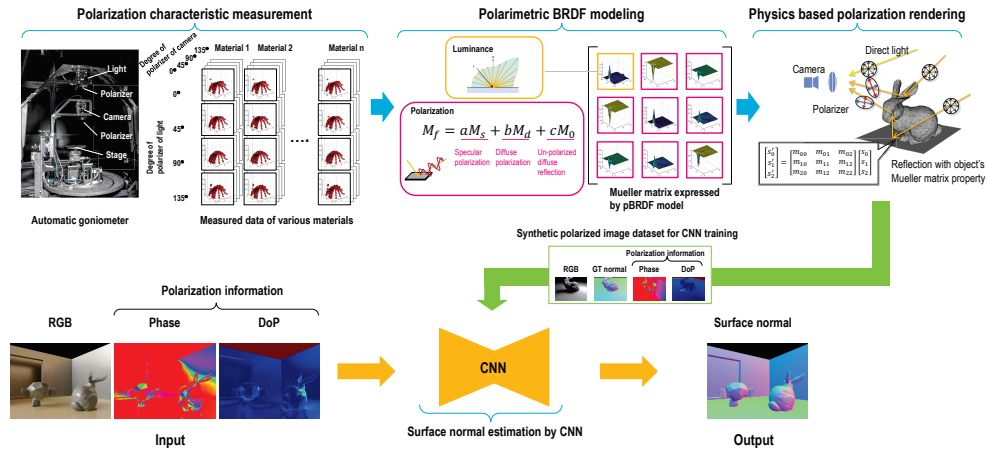


Fig. 1. Our framework: In order to create realistic polarized images, we build polarization-specific goniometer, and measure the polarization characteristic of materials with variety of light and camera conditions equipped with rotatable polarizers in front of them. Then, we estimate parameters of our polarimetric BRDF model by fitting our model to the measured data. After that, our polarization renderer simulates a large amount of synthetic polarized images reproducing polarization property by that model. Finally, synthetic polarized images are used to train CNN that estimates surface normal.

that only specular reflection is polarized, but as described in [12][36], diffuse reflection is also polarized in a different way from specular reflection. Since these two reflections are always mixed in real scenes, SfP is a very challenging task.

Kadambi et al. [16] used coarse depth map obtained from Microsoft Kinect to resolve ambiguity and fused coarse depth map and fine normal map to get fine depth map.

CNN is also used to solve these problems. Ba et al. [7] proposed that it is helpful to use polarized images to train Convolutional Neural Network (CNN) for surface normal estimation without ambiguity. Ba et al. [7] acquired polarized images and surface normal using a 3D scanner, and to increase the amount of training data, they synthesized polarized images from surface normal information. Although, as they simulate polarized images with diffuse reflection only, synthesized polarized images are quite different from real scene. To solve these problems, we also use CNN but with more accurately rendered data to train CNN. As shown in Fig. 1, the process consists of the following three steps,

- 1. Polarization Characteristic Measurement:** In order to obtain the polarization characteristic of real materials, we develop a measurement system which captures images with variety of light and camera positions and polarization angles.
- 2. Polarimetric BRDF Model:** In order to represent the polarization property for all incident/exitant light directions, we establish the generalized

polarimetric BRDF (pBRDF) model which can accurately describe actual polarization behavior for both specular and diffuse reflection.

- 3. Physics Based Polarization Rendering:** We develop a renderer which produces realistic polarized images using above model to train CNN.

We apply rendered polarized images to train CNN for surface normal estimation and show that with our synthesized dataset, estimated surface normal error is reduced by 70% compared to the one trained by RGB only.

2 Related Work

Polarization has long been studied in the computer vision field to understand the behavior of the reflectance of light. Wolff and Boult [35][36] showed the differences between specular polarization and diffuse polarization, and based on these differences, Nayar et al. [21] proposed a separation of specular reflection component and diffuse reflection component. As an application, Schechner et al. [28] demonstrated a haze removal using polarization. From the beginning of 2000, several studies related to the estimation of surface normal from polarization [1][3][5][19][20] and the polarization BRDF model [23][25][27][31] were proposed.

2.1 Shape from Polarization

In this section we describe SfP which estimates surface normal from the polarization information. Rahmann and Canterakis [24] estimated surface normal from the phase angle and the degree of polarization (DoP) of specular reflection. However, surface normal estimation from the polarization of specular reflection has azimuth and zenith ambiguity. To solve these ambiguity problems, Miyazaki et al. [20] and, Atkinson and Hancock [3] proposed surface estimation of dielectric objects by analyzing the polarization of diffuse reflection. In their work, the zenith angle obtained from DoP of diffuse reflection does not have an ambiguity, but the ambiguity of azimuth angle still remains. There are several works to solve the ambiguity problem: the fusion of polarization and depth map [13][16][41], multi-view camera with polarization [1][2][5][11][14][38], optimization using light distributions [20], shape from shading constraint [18][29], and photometric stereo with polarization [4][6][17][22].

As described in the previous section, the behaviors of specular and diffuse polarization are different, and both of them must be considered. Taamazyan et al. [30] proposed surface normal estimation with mixed polarization of specular and diffuse reflection. Baek et al, [8] explicitly defined the polarization of diffuse reflection in pBRDF model and estimate surface normal. Ba et al. [7] used CNN to obtain surface normal without ambiguity using polarized images and surface normal with ambiguity.

2.2 Polarimetric BRDF

Many pBRDF models have been proposed [15][23][26][31][34][40], but they ignore diffuse reflection component. There is a model which considers both specular and diffuse reflection [8], however, it assumes light source and camera are placed at the same optical axis. In this paper, we expand their pBRDF to correctly model arbitrary light and camera position.

3 Basics of Polarization

3.1 Surface Normal from Polarized Images

Intensity of the light $I(\phi_{pol})$ captured through a linear polarizer at an angle of ϕ_{pol} is expressed by the following equation.

$$I(\phi_{pol}) = \frac{I_{max} + I_{min}}{2} + \frac{I_{max} - I_{min}}{2} \cos(2(\phi_{pol} - \phi)) \quad (1)$$

We can infer three unknown variables (I_{max} , I_{min} , and ϕ) with more than three measurements at different polarization angles. DoP that represents how much the light is polarized, can be written as follows.

$$\rho = \frac{I_{max} - I_{min}}{I_{max} + I_{min}} \quad (2)$$

When the light is reflected by the surface, polarization state of the light changes depending on the surface angle. Therefore, by measuring polarization status of the light, one can estimate surface normal of the object.

Obtaining Surface Normal from Specular Reflection Component: When the observed light consists of specular reflection only, we can obtain surface normal (i.e. azimuth and zenith angle) with ambiguity from specular reflection component. The azimuth angle can be calculated from (1) and is $\phi + 90^\circ$. The zenith angle can be estimated from DoP with the following equation.

$$\rho^s = \frac{2 \sin^2 \theta \cos \theta \sqrt{\eta^2 - \sin^2 \theta}}{\eta^2 - \sin^2 \theta - \eta^2 \sin^2 \theta + 2 \sin^4 \theta} \quad (3)$$

where η denotes the refractive index and θ denotes the zenith angle.

Obtaining Surface Normal from Diffuse Reflection Component: Likewise, when the observed light consists of diffuse reflection only, we can obtain surface normal with ambiguity from the diffuse reflection component.

The zenith angle can be calculated from DoP using the following equation.

$$\rho^d = \frac{(\eta - 1/\eta)^2 \sin^2 \theta}{2 + 2\eta^2 - (\eta + 1/\eta)^2 \sin^2 \theta + 4 \cos \theta \sqrt{\eta^2 - \sin^2 \theta}} \quad (4)$$

Obtaining Surface Normal in the Real Scene: In real scenes, surface normal estimation becomes a very challenging task. We have two ambiguities in estimating azimuth angle. One is so called 180° ambiguity due to the fact that a polarizer can not distinguish between 0° and 180°. And the other is so called 90° ambiguity which is caused by mixed polarization of specular reflection and diffuse reflection. It is also difficult to obtain correct zenith angle, since the observed DoP is a mixture of two types of reflection.

3.2 Stokes Vector and Mueller Matrix

A Stokes vector is a four dimensional vector that represents the polarization state described as $\mathbf{s} = [s_0, s_1, s_2, s_3]^T$. s_0 is intensity of light, s_1 is the difference of 0° and 90° polarized intensity, s_2 is the difference of 45° and 135° polarized intensity and s_3 is the difference of right circular and left circular polarized intensity.

A Mueller matrix \mathbf{M} represents the change of the polarization state by reflection and refraction phenomena. When we define Stokes vectors before and after reflection/refraction as s and s' , their relationship is expressed as $s' = \mathbf{M}s$. When we omit circular polarization component, Mueller matrix is expressed as 3x3 matrix.

4 Our Polarimetric BRDF based on Measurement

In this section, we propose new pBRDF model which is applicable for arbitrary light and camera position.

4.1 Polarization Measurement System

We show our polarization characteristic measurement system in Fig. 1. To acquire polarization characteristics of various materials, we build an automated capturing system which can set the light and the camera with rotatable polarizers to arbitrary positions.

The Stokes vector observed in our system is expressed by the following equation.

$$\mathbf{s} = \begin{bmatrix} s_0 \\ s_1 \\ s_2 \end{bmatrix} = \begin{bmatrix} (I_0 + I_{45} + I_{90} + I_{135})/4 \\ (I_0 - I_{90})/2 \\ (I_{45} - I_{135})/2 \end{bmatrix} \quad (5)$$

$I_0, I_{45}, I_{90}, I_{135}$ are polarized intensities obtained by the camera with different polarizer angles.

The Stokes vectors obtained with different polarization angle of light, 0°, 45°, 90°, 135° are the followings.

$$\begin{bmatrix} s_0^{0^\circ} \\ s_1^{0^\circ} \\ s_2^{0^\circ} \end{bmatrix} = \mathbf{M} \begin{bmatrix} 1 \\ 1 \\ 0 \end{bmatrix} = \begin{bmatrix} m_{00} + m_{01} \\ m_{10} + m_{11} \\ m_{20} + m_{21} \end{bmatrix}, \quad \begin{bmatrix} s_0^{90^\circ} \\ s_1^{90^\circ} \\ s_2^{90^\circ} \end{bmatrix} = \mathbf{M} \begin{bmatrix} 1 \\ -1 \\ 0 \end{bmatrix} = \begin{bmatrix} m_{00} - m_{01} \\ m_{10} - m_{11} \\ m_{20} - m_{21} \end{bmatrix}$$

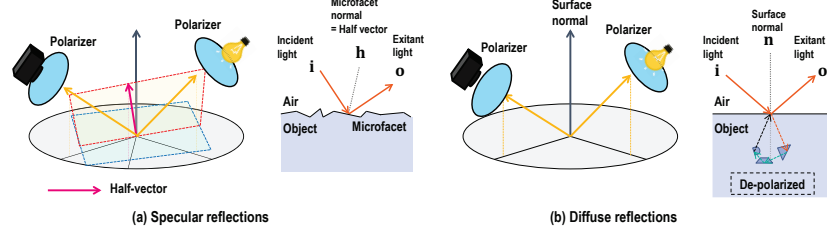


Fig. 2. Polarization of specular reflection and diffuse reflection : (a) Polarization of specular reflection is defined as the mirror-like reflection at the microfacet of the object. Incident light is reflected at the same angle to the half vector of light direction and camera direction. (b) Polarization of diffuse reflection is defined as the reflection that the light penetrate the material at first, depolarized inside the material, and then refracted back into the air.

$$\begin{bmatrix} s0^{45} \\ s1^{45} \\ s2^{45} \end{bmatrix} = \mathbf{M} \begin{bmatrix} 1 \\ 0 \\ 1 \end{bmatrix} = \begin{bmatrix} m00 + m02 \\ m10 + m12 \\ m20 + m22 \end{bmatrix}, \begin{bmatrix} s0^{135} \\ s1^{135} \\ s2^{135} \end{bmatrix} = \mathbf{M} \begin{bmatrix} 1 \\ 0 \\ -1 \end{bmatrix} = \begin{bmatrix} m00 - m02 \\ m10 - m12 \\ m20 - m22 \end{bmatrix} \quad (6)$$

We calculate Mueller matrices \mathbf{M} for each light and camera position. Using (6), Mueller matrices can be obtained in the following form.

$$\mathbf{M} = \begin{bmatrix} m00 & m01 & m02 \\ m10 & m11 & m12 \\ m20 & m21 & m22 \end{bmatrix} = \begin{bmatrix} \frac{s0^0 + s0^{90}}{2} & \frac{s0^0 - s0^{90}}{2} & \frac{s0^{45} - s0^{135}}{2} \\ \frac{s1^0 + s1^{90}}{2} & \frac{s1^0 - s1^{90}}{2} & \frac{s1^{45} - s1^{135}}{2} \\ \frac{s2^0 + s2^{90}}{2} & \frac{s2^0 - s2^{90}}{2} & \frac{s2^{45} - s2^{135}}{2} \end{bmatrix} \quad (7)$$

4.2 Polarimetric BRDF Model

In the previous work [8], pBRDF has been obtained for the camera and light which are fixed to coaxial position. Here, we describe our new pBRDF model which allows us to accurately model Mueller matrix for arbitrary camera and lighting position without any approximation.

Polarization of Specular Reflection. As shown in Fig. 2, in specular reflection, the incident light is reflected directly by the plane and its reflection angle can be described by the angle of incident light, camera direction and half vector. A half vector is described as: $\mathbf{h} = \frac{\mathbf{i} + \mathbf{o}}{\|\mathbf{i} + \mathbf{o}\|}$ where \mathbf{i} denotes the light direction and \mathbf{o} denotes the camera direction.

Generally, it is assumed that the plane is composed of many microfacets which have specular reflection property at different angle. The Mueller matrix of specular reflection is described as follows.

$$\mathbf{M}_{\mathbf{i}, \mathbf{o}}^s = \mathbf{C}_c(\phi_c) \mathbf{L}(\delta) \mathbf{R}(\theta_s; \eta) \mathbf{C}_l(\phi_l) \quad (8)$$

where $\mathbf{C}_l(\phi_l)$ denotes a rotation matrix of the angle ϕ_l from the polarizer axis of light into the incident plane, $\mathbf{R}(\theta_s; \eta)$ is the Fresnel term of specular reflection

that has the angle θ_s between a half vector \mathbf{h} and light \mathbf{i} , and η is the refractive index, and $\mathbf{L}(\delta)$ is a delay matrix. $\mathbf{C}_c(\phi_c)$ is a rotation matrix of the angle ϕ_c from the incident plane into the polarizer axis of a camera. $\mathbf{M}_{\mathbf{i},\mathbf{o}}^s$ can be denoted by the following matrix,

$$\mathbf{M}_{\mathbf{i},\mathbf{o}}^s = \begin{bmatrix} R^+ & R^- \gamma_l & R^- \chi_l & 0 \\ R^- \gamma_c & R^+ \gamma_l \gamma_c - R^\times \chi_l \chi_c \cos \delta & R^+ \chi_l \gamma_c + R^\times \gamma_l \chi_c \cos \delta & R^\times \chi_c \sin \delta \\ -R^- \chi_c & -R^+ \gamma_l \chi_c - R^\times \chi_l \gamma_c \cos \delta & -R^+ \chi_l \chi_c + R^\times \gamma_l \gamma_c \cos \delta & R^\times \gamma_c \sin \delta \\ 0 & R^\times \chi_l \sin \delta & -R^\times \gamma_l \sin \delta & R^\times \cos \delta \end{bmatrix} \quad (9)$$

With reference to [8], $\chi_{l,c} = \sin 2\phi_{l,c}$ and $\gamma_{l,c} = \cos 2\phi_{l,c}$. $R^+ = (R^p + R^s)/2$, $R^- = (R^s - R^p)/2$, and $R^\times = \sqrt{R^p R^s}$ are the Fresnel reflection coefficients. For dielectric objects, $\cos \delta = -1$ when the incident angle is less than Brewster angle. Otherwise $\cos \delta = 1$ and $\sin \delta = 0$. R^p, R^s are described as follows.

$$R^p = \left(\frac{\eta^2 \cos \theta_s - \sqrt{\eta^2 - \sin^2 \theta_s}}{\eta^2 \cos \theta_s + \sqrt{\eta^2 - \sin^2 \theta_s}} \right)^2, R^s = \left(\frac{\cos \theta_s - \sqrt{\eta^2 - \sin^2 \theta_s}}{\cos \theta_s + \sqrt{\eta^2 - \sin^2 \theta_s}} \right)^2 \quad (10)$$

Polarization of Diffuse Reflection. As illustrated in Fig. 2, diffuse reflection is observed when the light penetrates into the material, depolarized inside the material, and then refract back out to the air.

The Mueller matrix of diffuse reflection is described as follows.

$$\mathbf{M}_{\mathbf{i},\mathbf{o}}^d = \mathbf{C}_{\mathbf{nc}}(\phi_{\mathbf{nc}}) \mathbf{T}_{\mathbf{o}}(\theta_{\mathbf{o}}; \eta) \mathbf{P}_{\mathbf{o}} \mathbf{T}_{\mathbf{i}}(\theta_{\mathbf{i}}; \eta) \mathbf{C}_{\mathbf{ln}}(\phi_{\mathbf{ln}}) \quad (11)$$

$\mathbf{C}_{\mathbf{ln}}(\phi_{\mathbf{ln}})$ denotes the rotation matrix of the angle $\phi_{\mathbf{ln}}$ from the polarizer axis of light into the incident plane, $\mathbf{T}_{\mathbf{i}}(\theta_{\mathbf{i}}; \eta)$ is the Fresnel term of refraction from the air into the material surface, $\mathbf{P}_{\mathbf{o}}$ is a depolarization matrix, $\mathbf{T}_{\mathbf{o}}(\theta_{\mathbf{o}}; \eta)$ is the Fresnel term of refraction back out into the air, and $\mathbf{C}_{\mathbf{nc}}(\phi_{\mathbf{nc}})$ is a rotation matrix of the angle $\phi_{\mathbf{nc}}$ from the exitant plane into the polarizer axis of camera. In a depolarization matrix $\mathbf{P}_{\mathbf{o}}$, only $m00$ is 1 and the other elements are 0.

$$\mathbf{M}_{\mathbf{i},\mathbf{o}}^d = \begin{bmatrix} T_o^+ T_i^+ & T_o^+ T_i^- \beta_{ln} & T_o^+ T_i^- \alpha_{ln} & 0 \\ T_o^- T_i^+ \beta_{nc} & T_o^- T_i^- \beta_{ln} \beta_{nc} & T_o^- T_i^- \alpha_{ln} \beta_{nc} & 0 \\ -T_o^- T_i^+ \alpha_{nc} & -T_o^- T_i^- \beta_{ln} \alpha_{nc} & -T_o^- T_i^- \alpha_{ln} \alpha_{nc} & 0 \\ 0 & 0 & 0 & 0 \end{bmatrix} \quad (12)$$

$\alpha_{ln,nc} = \sin 2\phi_{ln,nc}$ and $\beta_{ln,nc} = \cos 2\phi_{ln,nc}$. $T_{i,o}^+ = (T_{i,o}^p + T_{i,o}^s)/2$, $T_{i,o}^- = (T_{i,o}^p - T_{i,o}^s)/2$ and $T_{i,o}^\times = \sqrt{T_{i,o}^p T_{i,o}^s}$ denoting the Fresnel transmission coefficients. We assume that the polarizer axis of the light and the camera are on the same incident and exitant plane, therefore $\mathbf{C}_{\mathbf{ln}}(\phi_{\mathbf{ln}})$ and $\mathbf{C}_{\mathbf{nc}}(\phi_{\mathbf{nc}})$ are identity

matrices and $\alpha_{ln,nc} = 0$, $\beta_{ln,nc} = 1$. $T_{i,o}^p, T_{i,o}^s$ are described as follows.

$$T_{i,o}^p = \frac{4\eta^2 \cos \theta_{i,o} \sqrt{\eta^2 - \sin^2 \theta_{i,o}}}{(\eta^2 \cos \theta_{i,o} + \sqrt{\eta^2 - \sin^2 \theta_{i,o}})^2}, T_{i,o}^s = \frac{4 \cos \theta_s \sqrt{\eta^2 - \sin^2 \theta_{i,o}}}{(\cos \theta_{i,o} + \sqrt{\eta^2 - \sin^2 \theta_{i,o}})^2} \quad (13)$$

Polarization Property Representation. As described above, our polarization characteristic measurement system captures only linear polarization since there is not much use of circular polarization in practice. Therefore, we only consider the top-left 3×3 Mueller matrix components that represent linear polarization. We estimate luminance parameters and polarization parameters separately. We normalize $\mathbf{M}^s, \mathbf{M}^d$ by their m_{00} components that represent the luminance:

$$\hat{\mathbf{M}}_{i,o}^s = \begin{bmatrix} 1 & -\rho^s \gamma_l & -\rho^s \chi_l \\ -\rho^s \gamma_c & \gamma_l \gamma_c - \frac{2R^\times}{R^+} \chi_l \chi_c \cos \delta & \chi_l \gamma_c + \frac{2R^\times}{R^+} \gamma_l \chi_c \cos \delta \\ \rho^s \chi_c & -\gamma_l \chi_c - \frac{2R^\times}{R^+} \chi_l \gamma_c \cos \delta & -\chi_l \chi_c + \frac{2R^\times}{R^+} \gamma_l \gamma_c \cos \delta \end{bmatrix} \quad (14)$$

$$\hat{\mathbf{M}}_{i,o}^d = \begin{bmatrix} 1 & \rho_i^d & 0 \\ \rho_o^d & \rho_o^d \rho_i^d & 0 \\ 0 & 0 & 0 \end{bmatrix} \quad (15)$$

where ρ^s and $\rho_{i,o}^d$ denote $(R^p - R^s)/(R^p + R^s)$ and $(T_{i,o}^p - T_{i,o}^s)/(T_{i,o}^p + T_{i,o}^s)$ that represent DoP in specular reflection and diffuse reflection.

We measure Mueller matrices of the material and express them as a linear combination of specular Mueller matrix and diffuse Mueller matrix. For each material and for each light and camera position, the normalized Mueller matrix $\mathbf{M}_{i,o}^f$ is described as follows.

$$\mathbf{M}_{i,o}^f = \mathbf{a}_{i,o} \hat{\mathbf{M}}_{i,o}^s + \mathbf{b}_{i,o} \hat{\mathbf{M}}_{i,o}^d + \mathbf{c}_{i,o} \mathbf{M}_0 \quad (16)$$

$$(a_{i,o} + b_{i,o} + c_{i,o} = 1)$$

$a_{i,o}, b_{i,o}, c_{i,o}$ are the coefficients for the single light and camera position. \mathbf{M}_0 is a depolarization matrix which represents diffraction and scattering of light inside materials. Finally, $\mathbf{M}_{i,o}^f$ is expressed as the following matrix.

$$\mathbf{M}_{i,o}^f = \begin{bmatrix} a + b + c & -a\rho^s \gamma_l + b\rho_i^d & -a\rho^s \chi_l \\ -a\rho^s \gamma_c + b\rho_o^d & a\gamma_l \gamma_c - a\frac{2R^\times}{R^+} \chi_l \chi_c \cos \delta + b\rho_o^d \rho_i^d & a\chi_l \gamma_c + a\frac{2R^\times}{R^+} \gamma_l \chi_c \cos \delta \\ a\rho^s \chi_c & -a\gamma_l \chi_c - a\frac{2R^\times}{R^+} \chi_l \gamma_c \cos \delta & -a\chi_l \chi_c + a\frac{2R^\times}{R^+} \gamma_l \gamma_c \cos \delta \end{bmatrix} \quad (17)$$

For each light and camera position, unknown variables are $a_{i,o}, b_{i,o}, c_{i,o}$, the specular DoP ρ^s , the diffuse DoP $\rho_{i,o}^d$ and $2R^\times/R^+$. These unknown variables

for each light and camera position can be estimated from the observed Mueller matrices.

From the observed Mueller matrices, we can calculate the specular DoP ρ^s and the diffuse DoP $\rho_{i,o}^d$ for each light and camera position from (17). Then, we estimate refractive index from DoPs using (3) and (4). $2R^\times/R^+$ can be obtained from estimated refractive index.

Finally, we estimate the linear combination coefficients $a_{\mathbf{i},\mathbf{o}}, b_{\mathbf{i},\mathbf{o}}, c_{\mathbf{i},\mathbf{o}}$.

BRDF Model with Polarization Property. We use the GGX BRDF model [33], to parameterize the luminance and polarization property $a_{\mathbf{i},\mathbf{o}}, b_{\mathbf{i},\mathbf{o}}, c_{\mathbf{i},\mathbf{o}}$. GGX model consists of the specular term and the diffuse term. The specular term takes into account Fresnel function, but the diffuse term does not. Therefore, we extend the diffuse term of the GGX model:

$$k^s \frac{D(\theta_h; \sigma) G(\theta_i, \theta_o; \sigma) F^s}{4(\mathbf{n} \cdot \mathbf{o})(\mathbf{n} \cdot \mathbf{i})} (\mathbf{n} \cdot \mathbf{i}) + (k^{pd} F^d + k^d)(\mathbf{n} \cdot \mathbf{i}) \quad (18)$$

where k^s, k^{pd} and k^d denote the coefficients for specular, polarized diffuse and un-polarized diffuse components. θ_h is the zenith angle between normal vector of the surface \mathbf{n} and half vector \mathbf{h} . θ_i and θ_o are the zenith angle between the normal vector \mathbf{n} and the light direction \mathbf{i} , and the camera direction \mathbf{o} respectively. σ is the surface roughness parameter of GGX distribution D . And G is the shadow/masking function. Fresnel coefficients are described as $F^s = R^+, F^d = T_o^+ T_i^+$ from $m00$ component of each Mueller matrix.

Here, parameterized coefficients of specular reflection and polarimetric diffuse reflection $\hat{a}_{\mathbf{i},\mathbf{o}}^s, \hat{b}_{\mathbf{i},\mathbf{o}}^{pd}$ are described as follows.

$$\hat{a}_{\mathbf{i},\mathbf{o}}^s = \frac{k^s \frac{DGF^s}{4(\mathbf{n} \cdot \mathbf{o})(\mathbf{n} \cdot \mathbf{i})} (\mathbf{n} \cdot \mathbf{i})}{k^s \frac{DGF^s}{4(\mathbf{n} \cdot \mathbf{o})(\mathbf{n} \cdot \mathbf{i})} (\mathbf{n} \cdot \mathbf{i}) + (k^{pd} F^d + k^d)(\mathbf{n} \cdot \mathbf{i})} \quad (19)$$

$$\hat{b}_{\mathbf{i},\mathbf{o}}^{pd} = \frac{k^{pd} F^d (\mathbf{n} \cdot \mathbf{i})}{k^s \frac{DGF^s}{4(\mathbf{n} \cdot \mathbf{o})(\mathbf{n} \cdot \mathbf{i})} (\mathbf{n} \cdot \mathbf{i}) + (k^{pd} F^d + k^d)(\mathbf{n} \cdot \mathbf{i})} \quad (20)$$

Now, we estimate GGX model parameters by solving an optimization problem that consists of three energy terms as follows.

$$E = E_a + \lambda_b E_b + \lambda_{lum} E_{lum} \quad (21)$$

$$E_a = \sum_{\mathbf{i},\mathbf{o}} \|a_{\mathbf{i},\mathbf{o}} - \hat{a}_{\mathbf{i},\mathbf{o}}^s\|_2^2, \quad E_b = \sum_{\mathbf{i},\mathbf{o}} \|b_{\mathbf{i},\mathbf{o}} - \hat{b}_{\mathbf{i},\mathbf{o}}^{pd}\|_2^2 \quad (22)$$

$$E_{lum} = \sum_{\mathbf{i},\mathbf{o}} \|m00_{\mathbf{i},\mathbf{o}} - (k^s \frac{DGF^s}{4(\mathbf{n} \cdot \mathbf{o})(\mathbf{n} \cdot \mathbf{i})} (\mathbf{n} \cdot \mathbf{i}) + (k^{pd} F^d + k^d)(\mathbf{n} \cdot \mathbf{i}))\|_2^2 \quad (23)$$

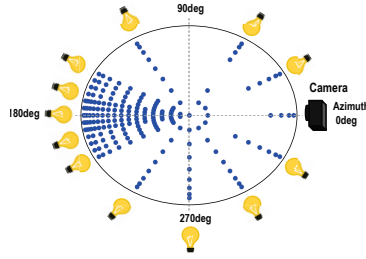


Fig. 3. Light positions: This is a top view of light positions at the camera azimuth 0° and zenith 30° . We measure the data in confronting positions densely. We lack some measurement points when the light source blocks the camera.

where E_a, E_b are for the polarization property, E_{lum} is the luminance property, and λ_b, λ_l are the weights. The weight of luminance depends on the captured intensity. We normalize luminance values by the maximum value in every material, but most values are very low when the material has sharp specular components. Therefore, we use $\lambda_b = 1, \lambda_l = 10^3$ as weights.

Finally, we obtain all parameters by optimization. In the optimization process, with reference to [9], first we estimate the diffuse parameters from the measured data without the data where the light and camera are in confronting position, after that, we estimate only specular parameters with the data where the light and camera are in confronting position.

4.3 Evaluation of Our Polarimetric BRDF

We compare our pBRDF model with Baek et al. [8] to evaluate the accuracy of refractive index estimation and Mueller matrix modeling. Note that the model [8] uses the data where the camera and light are at the coaxial position, while we use all measured data.

Measurement Setup. In this measurement, we assume the measured samples have isotropic BRDF, so the azimuth angle of the camera is fixed. Other parameters, the zenith angle of the camera, the azimuth and zenith angle of the light,

Table 1. Light and camera parameters in our system. (* Refer to Fig. 3.)

Parameters	Range	Number of positions
light azimuth	0:330	21 *
light zenith	0:85	9 or 18 *
light polarizer	0,45,90,135	4
camera azimuth	0 (fixed)	1
camera zenith	0:85	18
camera polarizer	0,45,90,135	4

and the rotation angle of polarizers in front of the light and camera are changed as described in Table 1. It shows the measurement positions and the polarizer angles of the light and the camera. Positions are not uniform as shown in Fig. 3. This is because the BRDF characteristics tend to change drastically when the light and the camera positions are at the confronting position, so dense measurements are necessary in that case. With this setup, we capture about 100,000 images for each material. For each captured image, 10x10 pixels in the center of image are averaged and used.

Evaluation of Refractive Index. We first evaluate the accuracy of the refractive index estimation for the materials with known refractive index value. The refractive index changes depending on the wavelength of the light, so we only use green channel data. Table 2 shows that our results are closer to the ground truth refractive index.

Table 2. Results of the refractive index estimation

Material	GT	Proposed	[8]
silicon nitride	2.0-2.1	2.09	2.00
alumina	1.75-1.80	1.76	1.58
aluminum nitride	2.1-2.2	1.99	1.58
zirconia	2.3-2.3	1.95	1.56
PVC	1.52-1.55	1.66	1.71
PTFE	1.35	1.55	1.51

Evaluation of Mueller Matrix. To evaluate accuracy of Mueller matrices represented by our pBRDF model, we first calculate output Stokes vectors by multiplying various Stokes vectors using modeled Mueller matrix. We use 24 different Stokes vectors that correspond to polarized images of $[0^\circ, 30^\circ, 60^\circ, 90^\circ, 120^\circ, 150^\circ]$ with the DoP of $[0, 0.25, 0.5, 1]$. And then, we convert output Stokes vectors back into luminance images. Obtained luminance values are compared with measured values to evaluate accuracy of our model. As illustrated in Fig. 4, we measure thirty different materials and evaluate the error between modeled values and observed values. Results show that our model represents variety of materials with less error. It follows that our pBRDF model can model luminance and polarization property of various materials even without the coaxial assumption.

In addition to the quantitative error evaluation of Mueller matrices, we evaluate the rendered image qualitatively. As shown in Fig. 5, the rendered image using our model is closer to the real image. This is because the model in [8] assumes the coaxial setup of the camera and the light, and can not represent the specular components correctly when the light position is separated from the camera position.

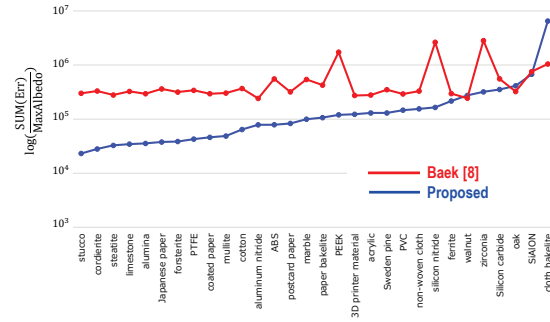


Fig. 4. Error of Mueller matrices for 30 materials: Proposed method and Baek [8] are compared. X-axis is measured materials and Y-axis is a sum of fitting errors with reference to [9]. Results are sorted by the error of proposed method.

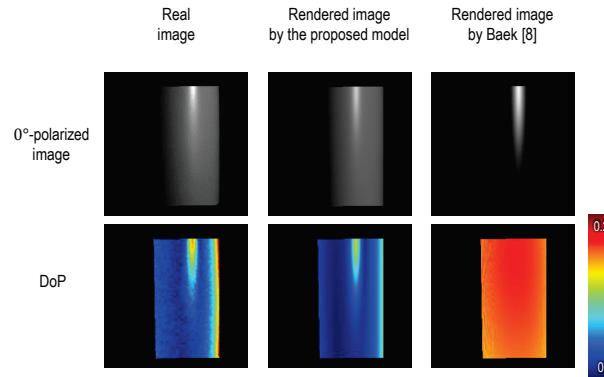


Fig. 5. Rendered results: We capture the cylinder object made of the 3D printer material in Fig. 4 and compare the 0° -polarized image and Degree of Polarization (DoP) by our model and Baek [8] to the real data.

5 Polarization Renderer

We build physics based renderer which can simulate the polarization behavior of rays based on the pBRDF of each material. In order to verify the accuracy of our polarization renderer, we set up real scene with objects whose polarization property and geometry information are known. In this evaluation, we first prepared a well-defined evaluation box and corresponding 3D model. The material characteristics of the evaluation box have been measured by our system, and to get fine geometry, we manually aligned the 3D mesh of the 3D printed Stanford bunny with the evaluation box on Blender. We rendered the same scene by our polarization renderer for comparison. Fig. 6 shows the result, the average PSNR between real image and rendered image is 29 dB for nine polarization angles. Our renderer can reproduce the polarization property correctly including interreflection effect in the real scenes.

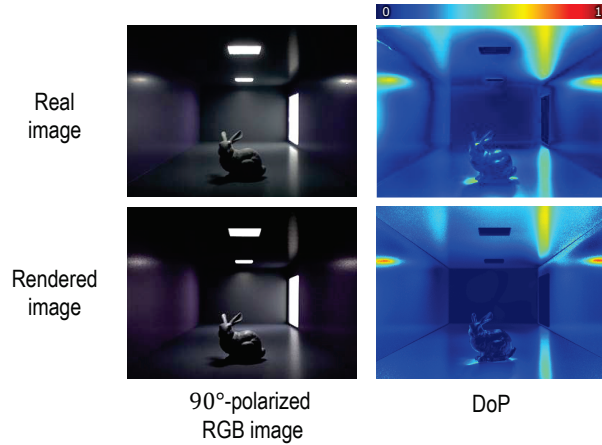


Fig. 6. Comparison between real image and rendered image: 90°-polarized image and the Degree of Polarization (DoP) is shown here.

6 Shape from Polarization by CNN Trained with Synthesized Polarization Images

Using a large number of rendered polarized images, we train CNN to estimate surface normal. In addition to RGB images, we use DoP and polarization phase derived from synthetic polarized images to train CNN.

To demonstrate the effectiveness of polarization information, we compare our surface normal results with Zhang et al. [39] which uses only the RGB images as input. Fig. 7 shows the comparison of the estimated surface normal for the synthetic data. Our proposed method estimate better surface normal for various materials and shapes.

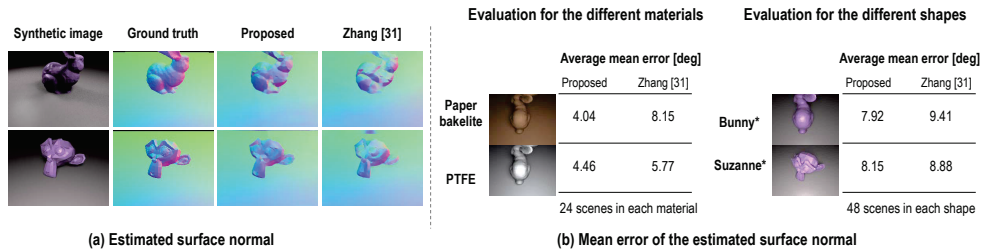


Fig. 7. Comparison of the estimated surface normal between our method and Zhang [39]. (a) Estimated surface normal images: The surface normal results by the proposed method using polarization information have less error. (b) Mean errors of the estimated surface normals: The proposed method estimates better surface normal for various materials and shapes. (*"Stanford Bunny" [32] and "Suzanne" [10])

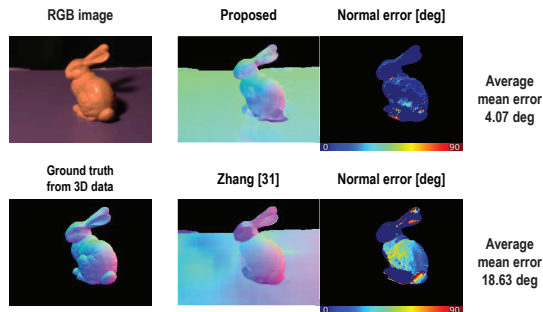


Fig. 8. Estimated surface normal for real scene by the proposed method and Zhang [39]. The ground truth of surface normal is manually adjusted 3D object data of Stanford Bunny[32].

Fig. 8 shows the comparison of estimated surface normal for the real data. Error of the estimated surface normal reduced by 70% with the proposed method.

Refer to the *supplementary material* for more details about our CNN architecture and training dataset.

7 Conclusion

In summary, we proposed the framework for utilizing polarization information of light. We first measured the polarization property of various materials, and modeled their polarization property using new pBRDF model that can describe polarization for omnidirectional setups of the cameras and lights. We made a renderer to generate a large number of realistic polarized images and used those images to train CNN for SfP task.

However, there are still some works that have to be done in our framework. Proposed pBRDF model can be extended to treat non-dielectric material and other materials which have anisotropic polarization reflectance property or more complex reflectance property. And, although the effectiveness of polarization information was shown for SfP task, other applications which can utilize polarization information more effectively should be studied. Since our framework can generate synthetic polarized images to train CNN, we believe that our framework can encourage people to seek for the new promising applications thanks to the power of CNN.

Acknowledgment We express our sincere thanks to our colleagues from Sony Corporation for their helpful discussion and support.

References

1. Atkinson, G.A., Hancock, E.R.: Multi-view surface reconstruction using polarization. In: IEEE International Conference on Computer Vision. vol. 1, pp. 309–316. IEEE (2005)
2. Atkinson, G.A., Hancock, E.R.: Polarization-based surface reconstruction via patch matching. In: IEEE Conference on Computer Vision and Pattern Recognition. vol. 1, pp. 495–502. IEEE (2006)
3. Atkinson, G.A., Hancock, E.R.: Recovery of surface orientation from diffuse polarization. *IEEE transactions on image processing* **15**(6), 1653–1664 (2006)
4. Atkinson, G.A., Hancock, E.R.: Recovering Material Reflectance from Polarization and Simulated annealing. In: Belhumeur, P., Ikeuchi, K., Prados, E., Soatto, S., Sturm, P. (eds.) *Proceedings of the First International Workshop on Photometric Analysis For Computer Vision - PACV 2007*. p. 8 p. INRIA, Rio de Janeiro, Brazil (Oct 2007), <https://hal.inria.fr/inria-00265255>, ISBN 2-7261-1297 8
5. Atkinson, G.A., Hancock, E.R.: Shape estimation using polarization and shading from two views. *IEEE transactions on pattern analysis and machine intelligence* **29**(11), 2001–2017 (2007)
6. Atkinson, G.A., Hancock, E.R.: Surface reconstruction using polarization and photometric stereo. In: *International Conference on Computer Analysis of Images and Patterns*. pp. 466–473. Springer (2007)
7. Ba, Y., Chen, R., Wang, Y., Yan, L., Shi, B., Kadambi, A.: Physics-based neural networks for shape from polarization. *arXiv preprint arXiv:1903.10210* (2019)
8. Baek, S.H., Jeon, D.S., Tong, X., Kim, M.H.: Simultaneous acquisition of polarimetric svbrdf and normals. *ACM Trans. Graph.* **37**(6), 268–1 (2018)
9. Bagher, M.M., Soler, C., Holzschuch, N.: Accurate fitting of measured reflectances using a shifted gamma micro-facet distribution. In: *Computer Graphics Forum*. vol. 31, pp. 1509–1518. Wiley Online Library (2012)
10. Blender: Suzanne. <https://www.blender.org/>, (Accessed: 15 Nov. 2019)
11. Chen, L., Zheng, Y., Subpa-Asa, A., Sato, I.: Polarimetric three-view geometry. In: *Proceedings of the European Conference on Computer Vision (ECCV)*. pp. 20–36 (2018)
12. Collett, E.: *Field Guide to Polarization*. Field Guide Series, SPIE Press (2005), <https://books.google.co.jp/books?id=5lJwcCsLbLsC>
13. Cui, Z., Gu, J., Shi, B., Tan, P., Kautz, J.: Polarimetric multi-view stereo. In: *IEEE Conference on Computer Vision and Pattern Recognition*. pp. 1558–1567 (2017)
14. Cui, Z., Larsson, V., Pollefeys, M.: Polarimetric relative pose estimation. In: *Proceedings of the IEEE International Conference on Computer Vision*. pp. 2671–2680 (2019)
15. Hyde Iv, M., Schmidt, J., Havrilla, M.: A geometrical optics polarimetric bidirectional reflectance distribution function for dielectric and metallic surfaces. *Optics express* **17**(24), 22138–22153 (2009)
16. Kadambi, A., Taamazyan, V., Shi, B., Raskar, R.: Polarized 3d: High-quality depth sensing with polarization cues. In: *IEEE International Conference on Computer Vision*. pp. 3370–3378 (2015)
17. Logothetis, F., Mecca, R., Sgallari, F., Cipolla, R.: A differential approach to shape from polarisation: A level-set characterisation. *International Journal of Computer Vision* **127**(11-12), 1680–1693 (2019)
18. Mahmoud, A.H., El-Melegy, M.T., Farag, A.A.: Direct method for shape recovery from polarization and shading. In: *IEEE International Conference on Image Processing*. pp. 1769–1772. IEEE (2012)

19. Miyazaki, D., Kagesawa, M., Ikeuchi, K.: Transparent surface modeling from a pair of polarization images. *IEEE Transactions on Pattern Analysis & Machine Intelligence* (1), 73–82 (2004)
20. Miyazaki, D., Tan, R.T., Hara, K., Ikeuchi, K.: Polarization-based inverse rendering from a single view. In: *IEEE International Conference on Computer Vision*. p. 982. IEEE (2003)
21. Nayar, S.K., Fang, X.S., Boult, T.: Separation of reflection components using color and polarization. *International Journal of Computer Vision* **21**(3), 163–186 (1997)
22. Ngo Thanh, T., Nagahara, H., Taniguchi, R.i.: Shape and light directions from shading and polarization. In: *IEEE Conference on Computer Vision and Pattern Recognition*. pp. 2310–2318 (2015)
23. Priest, R.G., Meier, S.R.: Polarimetric microfacet scattering theory with applications to absorptive and reflective surfaces. *Optical Engineering* **41** (2002)
24. Rahmann, S., Canterakis, N.: Reconstruction of specular surfaces using polarization imaging. In: *IEEE Conference on Computer Vision and Pattern Recognition*. vol. 1, pp. I–I. IEEE (2001)
25. Renhorn, I.G., Boreman, G.D.: Developing a generalized brdf model from experimental data. *Optics express* **26**(13), 17099–17114 (2018)
26. Renhorn, I.G., Hallberg, T., Bergström, D., Boreman, G.D.: Four-parameter model for polarization-resolved rough-surface brdf. *Optics express* **19**(2), 1027–1036 (2011)
27. Renhorn, I.G., Hallberg, T., Boreman, G.D.: Efficient polarimetric brdf model. *Optics express* **23**(24), 31253–31273 (2015)
28. Schechner, Y.Y., Narasimhan, S.G., Nayar, S.K.: Instant dehazing of images using polarization. In: *IEEE Conference on Computer Vision and Pattern Recognition*. pp. 325–332 (2001)
29. Smith, W.A., Ramamoorthi, R., Tozza, S.: Height-from-polarisation with unknown lighting or albedo. *IEEE transactions on pattern analysis and machine intelligence* **41**(12), 2875–2888 (2018)
30. Taamazyan, V., Kadambi, A., Raskar, R.: Shape from mixed polarization. *arXiv preprint arXiv:1605.02066* (2016)
31. Thilak, V., Voelz, D.G., Creusere, C.D.: Polarization-based index of refraction and reflection angle estimation for remote sensing applications. *Applied Optics* **46**(30), 7527–7536 (2007)
32. Turk, G., Levoy, M.: The stanford bunny. <http://graphics.stanford.edu/data/3Dscanrep/>, (Accessed: 15 Nov. 2019)
33. Walter, B., Marschner, S.R., Li, H., Torrance, K.E.: Microfacet models for refraction through rough surfaces. In: *Eurographics conference on Rendering Techniques*. pp. 195–206. Eurographics Association (2007)
34. Wang, K., Zhu, J.P., Liu, H.: Degree of polarization based on the three-component pbrdf model for metallic materials. *Chinese Physics B* **26**(2), 024210 (2017)
35. Wolff, L.B.: Polarization-based material classification from specular reflection. *IEEE transactions on pattern analysis and machine intelligence* **12**(11), 1059–1071 (1990)
36. Wolff, L.B., Boult, T.E.: Constraining object features using a polarization reflectance model. *IEEE Transactions on Pattern Analysis & Machine Intelligence* (7), 635–657 (1991)
37. Yamazaki, T., Maruyama, Y., Uesaka, Y., Nakamura, M., Matoba, Y., Terada, T., Komori, K., Ohba, Y., Arakawa, S., Hirasawa, Y., et al.: Four-directional pixel-wise polarization cmos image sensor using air-gap wire grid on 2.5- μm back-illuminated pixels. In: *IEEE International Electron Devices Meeting*. pp. 8–7. IEEE (2016)

38. Yang, L., Tan, F., Li, A., Cui, Z., Furukawa, Y., Tan, P.: Polarimetric dense monocular slam. In: Proceedings of the IEEE Conference on Computer Vision and Pattern Recognition. pp. 3857–3866 (2018)
39. Zhang, Y., Song, S., Yumer, E., Savva, M., Lee, J.Y., Jin, H., Funkhouser, T.: Physically-based rendering for indoor scene understanding using convolutional neural networks. In: IEEE Conference on Computer Vision and Pattern Recognition. pp. 5287–5295 (2017)
40. Zhang, Y., Zhang, Y., Zhao, H., Wang, Z.: Improved atmospheric effects elimination method for pbrdf models of painted surfaces. *Optics express* **25**(14), 16458–16475 (2017)
41. Zhu, D., Smith, W.A.: Depth from a polarisation + rgb stereo pair. In: IEEE Conference on Computer Vision and Pattern Recognition (2019)